Structural-mechanical remodelling of GDP-microtubules by kinesin

Daniel R. Peet[1,2], Nigel J. Burroughs[2,3], Robert A. Cross[1]*

[1]Centre for Mechanochemical Cell Biology, Warwick Medical School, Coventry, CV4 7AL, UK.

[2]Warwick Systems Biology Centre, University of Warwick, Coventry, CV4 7AL, UK.

[3]Mathematics Institute, University of Warwick, Coventry, CV4 7AL, UK.

Kinesin-1 is a nanoscale molecular motor that walks towards the fast growing (plus) ends of microtubules, hauling molecular cargo to specific reaction sites in cells. Kinesin-driven transport is central to the self-organisation of eukaryotic cells and shows great promise as a tool for nano-engineering[1,2]. Recent work hints that kinesin may also play a role in modulating the stability of its microtubule track, both *in vitro*[3-5] and *in vivo*[6], but results are conflicting[7-9] and mechanisms are unclear. Here we report a new dimension to the kinesin-microtubule interaction, whereby strong-state (ATP-bound and apo) kinesin-1 motor domains inhibit the shrinkage of dynamic microtubules by up to 2 orders of magnitude and expand their lattice spacing by ~1.6%. Our data reveal an unexpected new mechanism by which the mechanochemical cycles of kinesin and tubulin interlock, allowing motile kinesins to influence the structure, stability and mechanics of their microtubule track.

During stepping, kinesin motor domains cycle through a series of nucleotide-specific conformations[10,11]. We tested different nucleotide states of kinesin-1 motor domains to quantify their influence on microtubule stability. We attached fluorescent microtubule 'seeds' to the inside of a flow chamber via biotin-NeutrAvidin linkages and flowed in GTP-tubulin, causing dynamic microtubules to grow from the seeds (Fig. 1a). We then initiated microtubule depolymerisation by washing out tubulin, whilst simultaneously flowing in kinesin-1 motor domains. We used a kinesin motor domain mutant (T93N) as a stable homologue of the nucleotide-free (apo) state of the motor[12], and compared this to wild-type motor domains (K340) in the presence of different nucleotides. Strong-state kinesin binds tightly and stereospecifically to microtubules[13]. We found that T93N reduced microtubule shrinkage to 1% of the control rate (Fig. 1b,c) and that AMPPNP-WT kinesin had a similar effect, whilst weak-state (ADP-bound) kinesin had no detectable effect (Fig. 1c). We conclude that strong-state kinesin powerfully inhibits the shrinkage of GDP-microtubules.

Next, we bound microtubules to a kinesin-coated coverslip in a flow chamber, triggered depolymerisation by washing out residual GTP-tubulin, and again observed microtubule shrinkage. Geometric constraints suggest that in this arrangement, at most 5 protofilaments can bind to the kinesin surface (Fig. 2a). Despite this, entire microtubules were stabilised (Fig. 2c). We then flowed solutions through the channel in 2 steps (Fig. 2b). First, ADP was

flowed in, reducing the fraction of kinesins in a strong state and increasing the microtubule shrinkage rate (Fig. 2c, Supplementary Movie 1). By titrating the ADP concentration, we found that microtubule shrinkage rates could be fine-tuned over 2 orders of magnitude (Fig. 2d, Supplementary Table 1). Comparing the inhibition of microtubule shrinkage by kinesin in solution (maximally 0.21 ± 0.02 (25) dimer PF^{-1} s^{-1} (mean ± SEM (*n*))) with that of the kinesin surface (0.06 ± 0.01 (6) dimer PF^{-1} s^{-1} in the presence of 400 nM ADP) shows that surface immobilisation enhances the stabilising effect of kinesin, despite its binding being restricted to only a subset of protofilaments.

Frequently, faint fluorescent trails were visible on the kinesin-coated surface in the wake of retreating microtubule tips. These shrank endwise upon addition of ADP, suggesting that their tubulin is still assembled into protofilaments (Fig. 2c, Supplementary Movie 1). Trails are tapered, and fluorescence intensity analysis (Fig. 3a, Supplementary Methods and Supplementary Fig. 1-2) indicates that at their tips they contain 2-3 protofilaments (Fig. 3b). On average, trails can shrink faster than their microtubule stem because they appear transiently, typically forming, lengthening and retracting multiple times during the shrinkage of each surface-attached microtubule (Supplementary Fig. 3). As a final step in these experiments, we flowed in a buffer containing taxol and ATP, triggering kinesin-driven sliding to reveal the microtubule polarity.

Why does a kinesin-coated surface stabilise microtubules but also cause them to split? Several strands of evidence suggest that kinesin binding can change the lattice conformation and mechanics of MTs. A kinesin-coated surface has been reported to reduce the Young's modulus of taxol-stabilised microtubules[14]. Structural changes have also been reported for kinesin binding to taxol-stabilised microtubules[15]. More recent data has revealed significant kinesin-induced conformational changes in GMPCPP-microtubules[16]. Additionally, the longitudinal compaction of the microtubule lattice that accompanies GTP hydrolysis is

reduced in kinesin-bound microtubules[17], suggesting that kinesins can modify the longitudinal spacing between tubulin subunits in the microtubule lattice. We therefore hypothesised that kinesin binding changes the longitudinal spacing between GDP-tubulin subunits in the microtubule. Binding kinesins to one side of a microtubule would then change the lattice spacing on that side but not the other, causing shear stress.

To test the idea that kinesin binding stabilises a distinct conformation of the microtubule lattice, we used hydrodynamic flow to bend tethered dynamic microtubules, thereby expanding the microtubule lattice on the convex side and compressing it on the concave side (Fig. 4, Supplementary Movie 2). We supplemented T93N into the flow and observed the mechanical response of microtubules upon stopping the flow. In the absence of kinesins, the microtubules quickly recoiled to a straight conformation and rapidly depolymerised. Remarkably, low concentrations of T93N (15-30 nM) blocked this recoil, effectively locking the GDP-microtubules in a curved conformation as well as inhibiting their shrinkage. These data heavily suggest that indeed strong-state kinesins preferentially bind and stabilise a distinct longitudinal lattice spacing of GDP-microtubules.

In the presence of higher concentrations of kinesin (> 50 nM), the curved microtubules tended to slowly re-straighten. To explain this observation, we speculate that strong-state kinesins bind preferentially *but not exclusively* to one side of curved microtubules. At high kinesin concentrations, the favoured side of the microtubule would quickly become fully occupied, while binding would continue more slowly on the unfavoured side. This action would progressively reduce the asymmetry of kinesin binding, ultimately driving the microtubule back into a straight conformation (Fig. 4b). Kinesins have previously been reported to bind preferentially to GTP-microtubules, which have a longer lattice spacing than GDP-microtubules[18]. In light of this, we postulated that the binding of strong-state kinesins drives an increase in the lattice spacing of GDP-microtubules.

In order to directly test this model, we grew dynamic microtubules from surface-tethered fluorescent seeds as previously but this time capped their exposed tips with fluorescent GMPCPP-tubulin (Fig. 5a). We added methylcellulose at a concentration that causes microtubules to bind non-specifically to the surface at sparse interaction sites, so they stay in focus yet remain largely unrestrained. We then flowed in a high concentration (200 nM) of wild-type kinesin motor domains. As predicted, the GDP-bound (non-fluorescent) segment of the microtubule lengthened upon addition of apo-kinesin, bowing so as to adopt a longer path length between the surface-bound points (Fig. 5a, b; Supplementary Movie 3, Supplementary Fig. 5). Flowing in ADP releases the kinesin and allows the microtubule to recoil to its original length. This cycle appears fully reversible and can be repeated multiple times. Importantly, after the first cycle, microtubules became 'stitched' to the surface at more points than in the first cycle (Supplementary Movies 3 & 4), yet the measured expansion of the microtubule lattice spacing remains the same (Fig. 5c). We conclude that this technique is effective at restricting motion in the *z*-axis, thereby keeping microtubules in focus to allow for reliable measurement of their lengths, but it has no discernible effect on the kinesin-induced increase in lattice spacing.

Our data show that strong-state kinesin stabilises the GDP-lattice of dynamic microtubules, and concomitantly increases their lattice spacing by 1.6% (Fig. 5c). Kinesins are known to bind to the intra-dimer interface of αβ-tubulin, away from the inter-dimer contacts of the microtubule lattice[10,11,16,17]. This suggests to us that kinesin binding allosterically modifies the conformation of GDP-tubulin, giving it properties more similar to GTP-tubulin. Strong-state kinesins have previously been reported to alter the structure of both taxol-GDP-microtubules[15] and GMPCPP-microtubules[16]. Moreover, a long-range, ATP-dependent cooperative effect has been described whereby the first few kinesins that bind facilitate subsequent binding events in the same region of the microtubule, again suggestive of a kinesin-induced conformational change[19].

We envisage that the ability of strong-state kinesin to stabilise GDP-microtubules by inducing a conformational change in their tubulin subunits provides at least a partial mechanistic explanation for the surface-bound depolymerisation trails and the bend-locking phenomenon reported here. Thus, a microtubule landing on and binding to a kinesin-coated surface would likely become stretched on surface-bound side. This stretching would create shear stress in the lattice and potentially contribute towards formation of the trails observed in our kinesin-clamp experiments. Similarly, for the microtubule bend-locking, expanding the longitudinal microtubule lattice spacing by 1.6% exclusively on one side of the microtubule would be more than sufficient to account for the observed kinesin-stabilisation of curvature. Indeed, full occupancy on one side with zero occupancy on the other would produce a radius of curvature of 1.6 µm, far tighter than we observe in any of our post-flow data.

We have worked with kinesin-1, the best-studied kinesin, but it is possible that the mechanism we report here is common to other kinesins. Kif14 is a slow kinesin that binds to microtubules in a rigor-like conformation and inhibits their shrinkage[20]. Kinesin-5 is reported to stabilise protofilament assemblies during microtubule growth[21], potentially due to its strong state stabilising the polymer. Kip2[22] and Kip3[23] are also reported to dwell at microtubule ends and influence microtubule stability.

Our work reveals a specific action of strong-state kinesins in stabilising the GDP-lattice of dynamic microtubules. Microtubule activated ADP release creates a strong (apo) state and this process is affected by the tubulin and kinesin species[24], by post-translational modifications[25] and by the nucleotide state[26] of the microtubule. Importantly, the residency of kinesin in the strong states is also influenced by mechanical force[27]. Such forces will arise *in vivo* wherever kinesins do mechanical work, for example at kinetochores, in microtubule bundles[28], at cortical attachment sites[29], and during the transport of vesicles against a

resistance[30]. It will be important now to understand the role of these various effects in determining how kinesin motility may feed back on microtubule dynamics.

In conclusion, our data reveal a novel mechanism that allows kinesin-1 to feed back on the structure and stability of its microtubule track. Recent advances in the remote control of kinesin motility, such as photo-switchable fuels[31], suggest the potential for precise spatial control of these effects.

Methods

Proteins and biochemical reagents

Tubulin was purified from pig brains as previously[3] with additional steps as follows. Tubulin was polymerised in 50 mM PIPES, 1.2 mM $MgSO_4$, 1 mM EGTA, 1mM GTP, 1 mM dithiothreitol (DTT) and 186 mg ml^{-1} glutamic acid and incubated for 60 min at 37 °C. Microtubules were centrifuged in a TLA 100.3 rotor at 85,000 rpm for 20 min at 35 °C, resuspended in K-PEM with 1 mM GTP, 1 mM $MgSO_4$ and 1 mM DTT, cooled to 4 °C and centrifuged in a TLA 100.3 rotor at 85,000 rpm for 20 min. The supernatant was run through a Hiprep 26/10 desalting column into K-PEM buffer (100 mM PIPES, 1 mM $MgSO_4$, 2 mM EGTA (Fisher); adjusted to pH 6.9 with KOH) and 20 µM GTP. Tubulin concentrations were determined using E_{280} = 105,838 M^{-1} cm^{-1}.

X-rhodamine labelled tubulin was purchased from Cytoskeleton Inc. (USA). Alexa Fluor 488 (A-20000, Molecular Probes) labelled tubulin was prepared by reacting the dye with polymerised GTP-tubulin, removing unreacted dye by pelleting the microtubules at 4 °C, selecting for assembly-competent tubulin by polymerising and pelleting microtubules at 37 °C and again clarifying the solution by centrifugation at 4 °C[32].

Kinesin was purified as previously[33]. Kinesin concentrations were determined using E_{280} = 15,300 M^{-1} cm^{-1}.

Nucleotides were from Jena Biosciences (Germany). Other reagents were from Sigma (UK).

Flow chamber assembly

Flow chambers were assembled from 22x22 mm no. 1.5 glass coverslips (Menzel, Germany) and 76x26 mm 1-1.2 mm thickness glass slides (Menzel, Germany). Double-sided Scotch tape was sandwiched between the glass surfaces to form a 2 mm wide channel. The

170 periphery of the chamber was further secured using nail polish excluding the channel ends,
171 which were left open. Solutions were drawn through the channel by using grade 1 Whatman
172 filter paper.

173 **Tubulin depletion and microtubule bending assay**

174 Coverslips were sonicated (600 W bath, Ultrawave) in 3% Neutracon detergent (Decon
175 Laboratories, UK) for 30 min at 60 °C before undergoing extensive wash-sonication cycles in
176 ultrapure water (18.2 MΩ cm resistivity). A flow chamber was then assembled, filled with
177 0.2 mg ml^{-1} PLL-PEG-biotin (SuSoS, Switzerland) and incubated for 30 min. The chamber was
178 washed with K-PEM before adding 1 mg ml^{-1} NeutrAvidin (Thermo Fisher Scientific) for 5 min
179 and washing again. Microtubule seeds (polymerised by incubating 26 µM tubulin and 1 mM
180 GMPCPP in K-PEM at 37 °C for 25 min) were pelleted, diluted to ~ 60 nM, injected into the
181 chamber and incubated for 5 min. After washing the chamber with K-PEM, dynamic
182 microtubule extensions were grown from the seeds by flowing through with 15 µM tubulin,
183 1 mM GTP, GOC oxygen scavenger (4.5 mg ml^{-1} glucose, 0.2 mg ml^{-1} glucose oxidase, 35 µg
184 ml^{-1} catalase, 0.5% (v/v) β-mercaptoethanol), 1 mg ml^{-1}, 1 mg ml^{-1} BSA and 0.1% (v/v)
185 Tween20 in K-PEM. Microtubules were allowed to grow for > 15 min at 25 °C prior to
186 imaging. Tubulin was then depleted by flowing through pre-warmed (25 °C) K-PEM,
187 supplemented with kinesin motor domains and nucleotides as described in the main text.
188 Microtubule bending was achieved by rapidly drawing solutions through the channel using
189 Whatman filter paper.

190 **Kinesin-clamp assay**

191 Fluorescence controls (colour-segmented stabilised microtubules) were prepared by
192 incubating 5 µM 30% labelled Alexa Fluor 288 tubulin and 0.2 mM Guanosine-5'-[(α,β)-
193 methyleno]triphosphate (GMPCPP) in K-PEM at 37 °C for 60 min and pelleted in an airfuge

(Beckman Coulter) at 25 psi for 10 min. The supernatant was discarded and the pellet resuspended in pre-warmed 5 µM 30% labelled X-rhodamine tubulin and 0.2 mM GMPCPP in K-PEM. Microtubules were left to anneal at room temperature then diluted 50-fold before use.

Coverslips were sonicated (600 W bath) at room temperature in a 1:1 solution of methanol and HCl for 30 min, then sonicated for 4 × 5 min in ultrapure water. Coverslips were then sonicated in 0.2 M KOH for 60 min, then sonicated for 5 × 5 min in ultrapure water. The coverslips were then spun dry using a Spin Clean (Technical video), incubated at 100 °C for 30 min and plasma-cleaned (PLASMA clean 4, ILMVAC) for 5 min. Coverslips were then silanised by immersion in 0.05% dimethyldichlorosilane in trichloroethylene for 60 min, washed in methanol, sonicated for 5 × 5 min in methanol and spun dry.

A flow chamber was assembled using a silanised coverslip and filled with 0.1 mg ml^{-1} anti-6xHistidine antibodies (372900) for 10 min. The surface was then blocked by filling the chamber with 0.5 mg ml^{-1} α-casein and incubating for 5 min. 75 nM K340 was then introduced and incubated for 10 min, after which the chamber was washed with 10 chamber volumes of K-PEM. Stabilised segmented microtubules were then introduced. Unbound microtubules were washed out immediately with K-PEM. Dynamic microtubules, polymerised by incubating 50 µM 30% labelled Alexa Fluor 488 tubulin (same stock as used for fluorescence controls) and 1 mM GTP in K-PEM for 45 min at 37 °C, were diluted 20-fold in warm (37 °C) K-PEM and immediately flowed through the chamber. Next, 10 chamber volumes of warm K-PEM were flowed rapidly through the chamber. The sample was then imaged and ADP in K-PEM was introduced at the desired concentration. Once microtubules had shortened sufficiently, 10 µM taxol and 200 µM ATP in K-PEM was flowed into the chamber.

Lattice spacing-change assay

Coverslips were incubated in 1 M HCl at 50 °C for 12-15 hours, rinsed with ultrapure water twice, sonicated in ultrapure water for 30 min, sonicated in ethanol for 30 min, rinsed in ethanol and dried by spinning or spraying with nitrogen gas. Microtubules were then polymerised following the same initial steps as the tubulin depletion assay, except the fluorescent labelling ratio of the tubulin used for seeds was 30% and the dynamic extensions were grown using 20 µM tubulin. Microtubules were capped after 45-60 min by flowing 6 µM of 30% Alexa Fluor 488 labelled tubulin and 1 mM GMPCPP in K-PEM for 10 min before washing the chamber with 100 µl of 0.1% Tween in K-PEM. Hereafter, each buffer contained GOC, 0.1% Tween20 and 0.02% methylcellulose (Sigma, 4000 cP) in K-PEM. The chamber was washed with 30 µl of buffer before imaging. During imaging, 40 µl of 200 nM K340 was flowed through, followed later by 40 µl of 1 mM ADP. Flowing through 100 µl of buffer depleted the ADP, after which a new field of view could be imaged and the kinesin & ADP flows repeated. We imaged no more than five times in a single flow channel.

Microscopy

Images were captured by an EM-CCD camera (iXon^{EM}+DU-897E, Andor) fitted to a Nikon E800 microscope with a Plan Fluor 100x NA 0.5-1.3 variable iris objective. A custom-built enclosure with an air heater (Air-Therm ATX, World Precision Instruments) was used to keep samples at 25 °C. Dark-field illumination was achieved using a 100 W mercury lamp connected to the microscope via a fibre optic light scrambler (Technical video), cold mirror, 500-568 nm band-pass filter (Nikon) and a dark-field condenser (Nikon). A stabilised mercury lamp (X-cite exacte, Lumen Dynamics) provided illumination for epifluorescence, connected to the microscope with a light pipe. Motorised filter wheels (Ludl Electronic Products) housed the fluorescence excitation and emission filters: 485/20 and 536/40 for Alexa-488 and 586/20 and 628/32 for X-rhodamine (Chroma). Combined dark-field and fluorescence imaging was achieved using an FF505/606-Di01-25x36 dichroic mirror (Semrock) and

244 electronic shutters to switch between illumination modes. The shutters, filter wheels and
245 camera were controlled using Metamorph software (Molecular Devices).

246 **Kymograph analysis**

247 Data were analysed in Matlab (Mathworks). Each microtubule image was aligned
248 horizontally, using the function *imrotate* to rotate the image according to a hand-drawn line,
249 before averaging columns of 11 pixels spanning the microtubule to generate an intensity
250 profile. This was repeated for the same region of interest (ROI) for every frame in an image
251 stack. Kymographs were produced by vertically concatenating the intensity profiles.
252 Shrinkage rates were measured by manually tracing kymographs using the impoly function,
253 extracting coordinates and calculating the slope. Time and distance calibration was
254 automated by extracting the image metadata. Rates quoted in this paper assume a
255 conversion of 125 dimer PF^{-1} = 1 µM. Quantitative fluorescence analysis of microtubules in a
256 kinesin-clamp is presented in Supplementary Methods. Graph plotting and statistical tests
257 were also carried out using Matlab.

258 **Analysis of microtubule lattice spacing changes**

259 Coordinates of microtubules were extracted from dark-field images using the semi-
260 automated ImageJ plugin, JFilament[34]. The coordinates were then mapped onto the
261 fluorescence channel and used to generate a 5-pixel-wide line scan. The fluorescence
262 profiles of the cap and the seed were each fitted with a Gaussian error function in Matlab.
263 The length of the GDP-bound section of the microtubule is then given by the distance
264 between the point of inflection on each curve. The microtubule length change was then
265 assessed by taking the mean length of the manually identified plateaus, as shown in Fig. 5c.
266 Points deviating by greater than 5% from the median length in these intervals were
267 discarded prior to fitting. Long microtubules were selectively chosen for the analysis to
268 improve precision, with the average length of kinesin-free GDP-microtubule segments being

269 41 µm.

References

1. Goel, A. & Vogel, V. Harnessing biological motors to engineer systems for nanoscale transport and assembly. *Nature Nanotech* **3,** 465–475 (2008).
2. Bachand, G. D., Spoerke, E. D. & Stevens, M. J. Microtubule-based nanomaterials: Exploiting nature's dynamic biopolymers. *Biotechnology and Bioengineering* **112,** 1065–1073 (2015).
3. Katsuki, M., Drummond, D. R. & Cross, R. A. Ectopic A-lattice seams destabilize microtubules. *Nature Communications* **5,** 3094 (2014).
4. Lombillo, V. A., Stewart, R. J. & McIntosh, J. R. Minus-end-directed motion of kinesin-coated microspheres driven by microtubule depolymerization. *Nature* **373,** 161–164 (1995).
5. Dumont, E. L. P., Do, C. & Hess, H. Molecular wear of microtubules propelled by surface-adhered kinesins. *Nature Nanotech* **10,** 166–169 (2015).
6. Marceiller, J., Drechou, A., Durand, G., Perez, F. & Poüs, C. Kinesin is involved in protecting nascent microtubules from disassembly after recovery from nocodazole treatment. *Exp. Cell Res.* **304,** 483–492 (2005).
7. Kowalski, R. J. & Williams, R. C. Unambiguous classification of microtubule-ends in vitro: Dynamic properties of the plus- and minus-ends. *Cell Motility and the Cytoskeleton* **26,** 282–290 (1993).
8. Daire, V. *et al.* Kinesin-1 regulates microtubule dynamics via a c-Jun N-terminal kinase-dependent mechanism. *Journal of Biological Chemistry* **284,** 31992–32001 (2009).
9. Kimura Arimura Fukata, T. N. Y., Watanabe, H., Iwamatsu, A. & Kaibuchi, K. Tubulin and CRMP-2 complex is transported via Kinesin-1. *Journal of Neurochemistry* **93,** 1371–1382 (2005).
10. Atherton, J. *et al.* Conserved mechanisms of microtubule-stimulated ADP release, ATP binding, and force generation in transport kinesins. *eLife* **3,** e03680 (2014).
11. Shang, Z. *et al.* High-resolution structures of kinesin on microtubules provide a basis for nucleotide-gated force generation. *eLife* **3,** e04686 (2014).
12. Nakata, T. & Hirokawa, N. Point mutation of adenosine triphosphate-binding motif generated rigor kinesin that selectively blocks anterograde lysosome membrane transport. *J Cell Biol* **131,** 1039–1053 (1995).
13. Cross, R. A. The kinetic mechanism of kinesin. *Trends Biochem. Sci.* **29,** 301–309 (2004).
14. Kabir, A. M. R. *et al.* Biomolecular Motor Modulates Mechanical Property of Microtubule. *Biomacromolecules* **15,** 1797–1805 (2014).
15. Krebs, A., Goldie, K. N. & Hoenger, A. Complex formation with kinesin motor domains affects the structure of microtubules. *Journal of Molecular Biology* **335,** 139–153 (2004).
16. Morikawa, M. *et al.* X-ray and Cryo-EM structures reveal mutual conformational changes of Kinesin and GTP-state microtubules upon binding. *The EMBO Journal* **34,** 1270–1286 (2015).
17. Alushin, G. M. *et al.* High-Resolution Microtubule Structures Reveal the Structural Transitions in αβ-Tubulin upon GTP Hydrolysis. *Cell* **157,** 1117–1129 (2014).
18. Nakata, T., Niwa, S., Okada, Y., Perez, F. & Hirokawa, N. Preferential binding of a kinesin-1 motor to GTP-tubulin-rich microtubules underlies polarized vesicle transport. *The Journal of Cell Biology* **194,** 245–255 (2011).
19. Muto, E. E., Sakai, H. H. & Kaseda, K. K. Long-range cooperative binding of kinesin to a microtubule in the presence of ATP. *J Cell Biol* **168,** 691–696 (2005).

20. Arora, K. *et al.* KIF14 binds tightly to microtubules and adopts a rigor-like conformation. *Journal of Molecular Biology* **426,** 2997–3015 (2014).
21. Chen, Y. & Hancock, W. O. Kinesin-5 is a microtubule polymerase. *Nature Communications* **6,** 8160 (2015).
22. Hibbel, A. *et al.* Kinesin Kip2 enhances microtubule growth in vitro through length-dependent feedback on polymerization and catastrophe. *eLife* **4,** e10542 (2015).
23. Varga, V., Leduc, C., Bormuth, V., Diez, S. & Howard, J. Kinesin-8 motors act cooperatively to mediate length-dependent microtubule depolymerization. *Cell* **138,** 1174–1183 (2009).
24. Alonso, M. C. *et al.* An ATP Gate Controls Tubulin Binding by the Tethered Head of Kinesin-1. *Science* **316,** 120–123 (2007).
25. Sirajuddin, M., Rice, L. M. & Vale, R. D. Regulation of microtubule motors by tubulin isotypes and post-translational modifications. *Nature Cell Biology* **16,** 335–344 (2014).
26. Vale, R. D., Coppin, C. M., Malik, F., Kull, F. J. & Milligan, R. A. Tubulin GTP hydrolysis influences the structure, mechanical properties, and kinesin-driven transport of microtubules. *Journal of Biological Chemistry* **269,** 23769–23775 (1994).
27. Carter, N. J. & Cross, R. A. Mechanics of the kinesin step. *Nature* **435,** 308–312 (2005).
28. Cross, R. A. & McAinsh, A. Prime movers: the mechanochemistry of mitotic kinesins. *Nature Reviews Molecular Cell Biology* **15,** 257–271 (2014).
29. Hendricks, A. G. *et al.* Dynein Tethers and Stabilizes Dynamic Microtubule Plus Ends. *Current Biology* **22,** 632–637 (2012).
30. Blehm, B. H., Schroer, T. A., Trybus, K. M., Chemla, Y. R. & Selvin, P. R. In vivo optical trapping indicates kinesin's stall force is reduced by dynein during intracellular transport. *PNAS* **110,** 3381–3386 (2013).
31. Perur, N., Yahara, M., Kamei, T. & Tamaoki, N. A non-nucleoside triphosphate for powering kinesin-microtubule motility with photo-tunable velocity. *Chem. Commun.* **49,** 9935–9937 (2013).
32. Katsuki, M., Muto, E. & Cross, R. A. *Microtubule Dynamics*. **777,** 117–126 (Humana Press, 2011).
33. Crevel, I. *et al.* What kinesin does at roadblocks: the coordination mechanism for molecular walking. *The EMBO Journal* **23,** 23–32 (2004).
34. Smith, M. B. *et al.* Segmentation and tracking of cytoskeletal filaments using open active contours. *Cytoskeleton* **67,** 693–705 (2010).

Acknowledgements

The authors thank D. R. Drummond and N. Sheppard for assistance with protein purification, and T. A. McHugh for invaluable comments on the manuscript. This research was funded by the Biotechnology and Biological Sciences Research Council (grant number BB-G530233-1) via the Systems Biology Doctoral Training Centre, University of Warwick; and the Wellcome Trust (grant number 103895/Z/14/Z).

Author contributions

D.R.P. and R.A.C. designed experiments. N.J.B. provided mathematical insight. D.R.P. collected and analysed the data, and produced the manuscript and figures. All authors contributed towards the discussion and interpretation of results, and editing the manuscript.

Competing financial interests

The authors declare no competing financial interests.

Figure legends

Supplementary Movie 1 | A kinesin-clamp assay. The image data (*top*) corresponds to the kymograph in Fig. 2c (*bottom*). A minus-end trail is clearly seen in the no nucleotide phase. Addition of ADP causes the microtubule tips to shrink. In this case, the minus-end trail is retained during shrinkage. Microtubules are re-stabilised upon addition of taxol and ATP, and the resulting kinesin-driven microtubule gliding reveals the microtubule polarity.

Supplementary Movie 2 | Strong-state kinesin can lock the curvature of GDP-microtubules. For each concentration of T93N, images are sorted according to the microtubule orientation. The marked microtubules in each row (*orange asterisks*) fall into the orientation range depicted by the protractor diagrams (*left*). Microtubules are straight and dynamically unstable at the beginning of the movie. Arrows (*top*) highlight the presence and direction of hydrodynamic flow, which causes microtubule bending. In the absence of kinesin, stopping the flow causes the microtubules to re-straighten and continue to depolymerise. Microtubule curvature is preserved at low concentrations of T93N but mitigated at high concentrations.

Supplementary Movie 3 | Kinesin binding reversibly increases the lattice spacing of GDP-microtubules. The movie corresponds to the microtubule shown in Fig. 5a. Part way through the movie, 200 nM of monomeric kinesin (K340) is flowed through the channel and the microtubule extends and bends so as to follow a longer path length. Flushing with 1 mM ADP triggers kinesin unbinding, and the microtubule reverts to its original length. After washing the sample thoroughly with buffer, the process can be repeated. After the first cycle, the microtubule becomes tethered to the surface at a greater number of interaction sites. During the second kinesin flow-through, part of the microtubule briefly goes out of focus but it is recruited back into the optical plane, demonstrating that our protocol restricts

396 motion in the *z*-axis to permit reliable quantification. Scale bar is 10 µm.

397

398 **Supplementary Movie 4 | A fourth cycle of kinesin-induced microtubule lattice expansion.**

399 Kinesin and ADP were flowed through as in Supplementary Movie 3 but the microtubule

400 shown is undertaking its fourth expansion-contraction cycle. It is clearly well-confined to the

401 surface because it remains fully in focus throughout the duration of the movie, yet lattice

402 expansion occurs to the same extent as in earlier cycles. Scale bar is 10 µm.

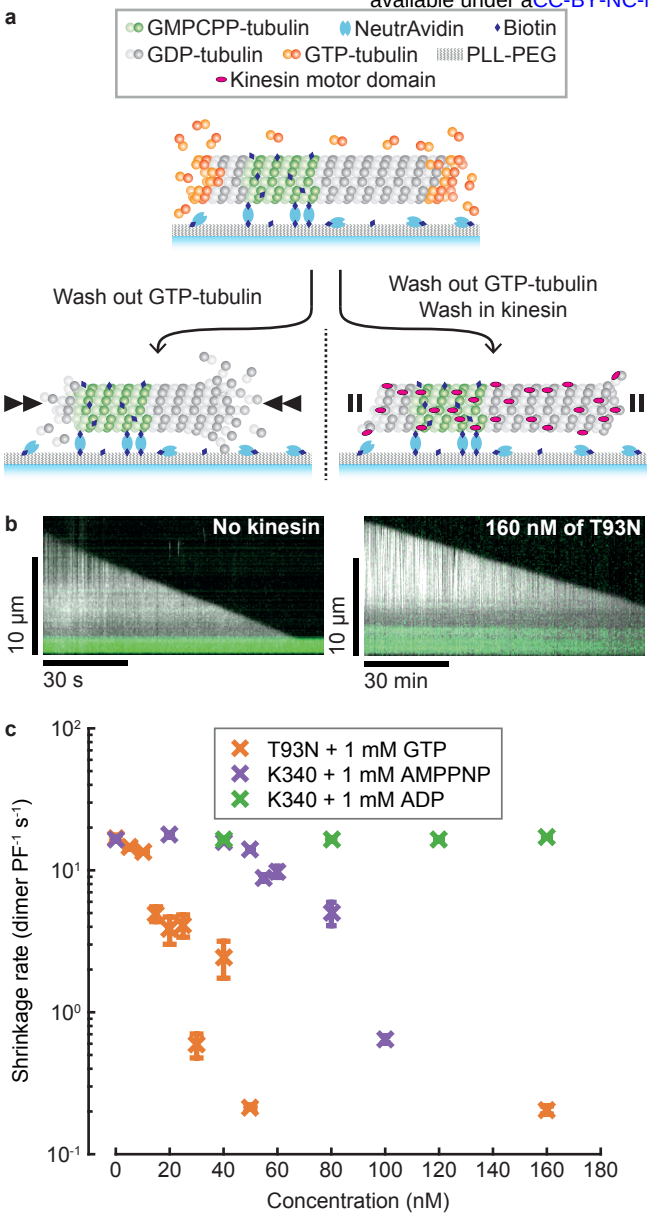

Figure 1 | Strong-state kinesins inhibit GDP-microtubule shrinkage. a, Schematic representation of a tubulin depletion assay. Dynamic microtubules shrink rapidly when GTP-tubulin is depleted (left) unless bound to strong-state kinesins (right). **b,** Representative kymographs of microtubules shrinking in the absence (left) and presence (right) of T93N. Note the different time scales. Dynamic microtubules are shown in white (dark-field) and fluorescent seeds in green (epi-fluorescence). **c,** Shrinkage rates of microtubules bound to kinesins in distinct nucleotide states. GTP was included with T93N only. Error bars are mean ± SEM. $14 \leq n \leq 53$ for all conditions.

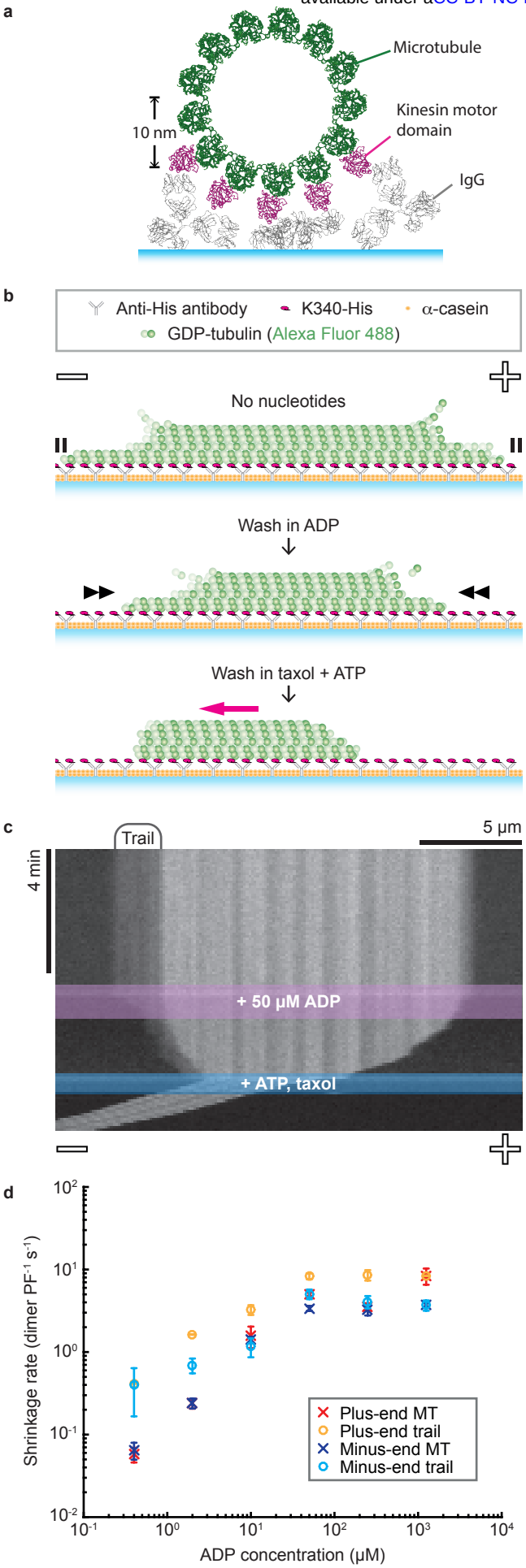

Figure 2 | Microtubules are stabilised when kinesins bind to one side of the lattice. a, Cross-sectional view of a kinesin-clamp assay, showing IgG (PDB:1IGY) and kinesin-bound microtubule (PDB:4UXT) structures to provide scale. **b,** Schematic of a kinesin-clamp assay. **c,** Representative kymograph of a microtubule in a kinesin-clamp. **d,** Average shrinkage rates of microtubules and their trails. Error bars are mean ± SEM, reflecting inter-microtubule variability. *n*-values are given in Supplementary Table 1.

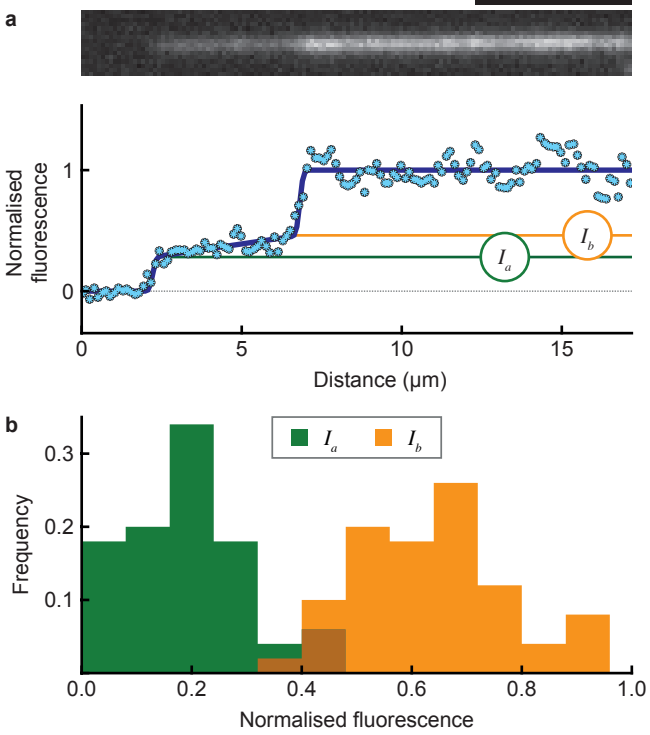

Figure 3 | Subsets of protofilaments are stabilised by a kinesin-coated surface. a, Model fit to the intensity profile of a microtubule tip (bottom) with the associated fluorescence image (top). (I_a) is the intensity at the tip and (I_b) at the base of the trail. Scale bar: 5 μm. b, Histogram of (I_a) and (I_b) values for (n = 50) microtubules, normalised to the intensities of their parent microtubules in the no-nucleotide phase of the experiment. Mean ± standard deviation is 0.19 ± 0.11 and 0.64 ± 0.13 for I_a and I_b, respectively.

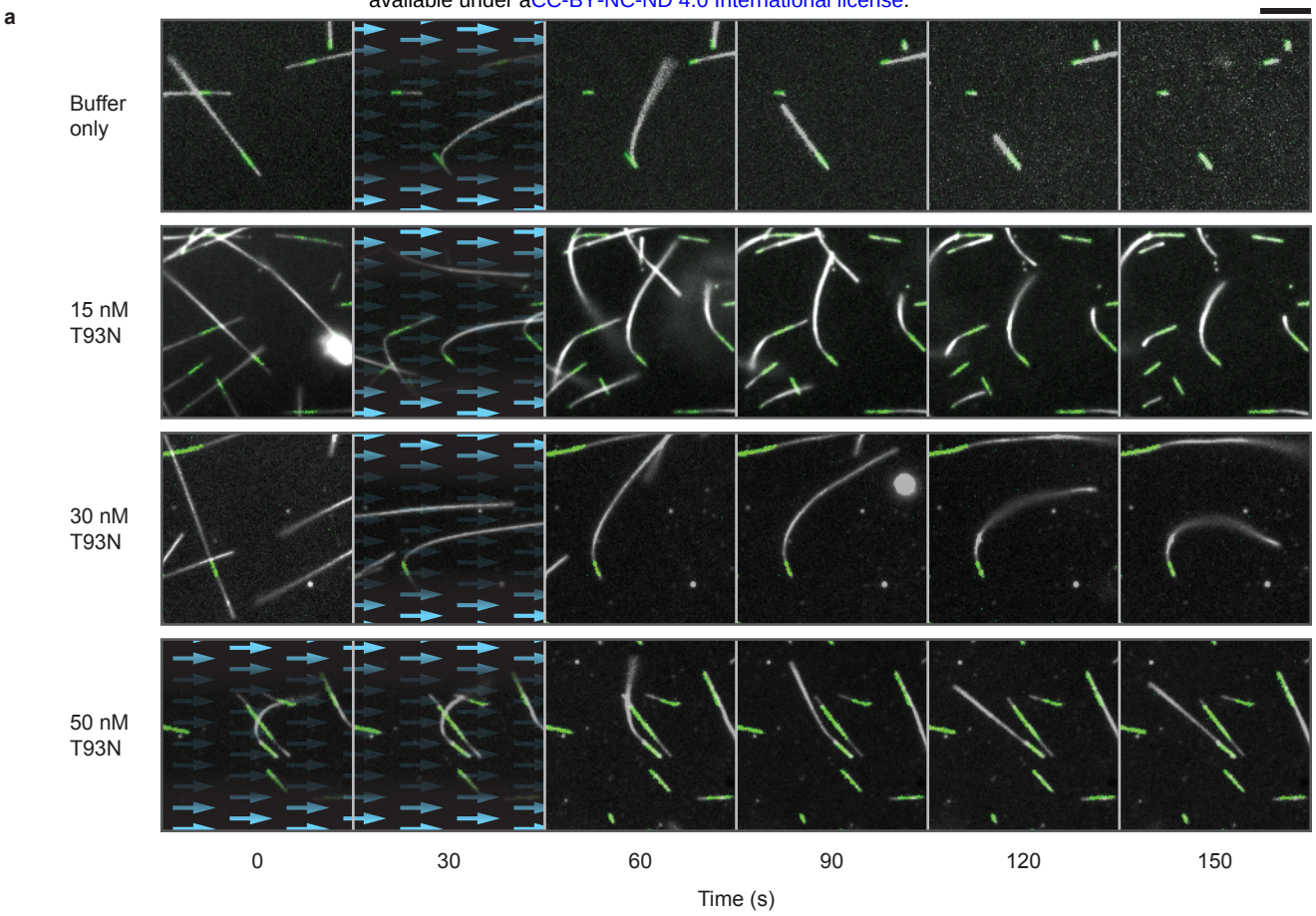

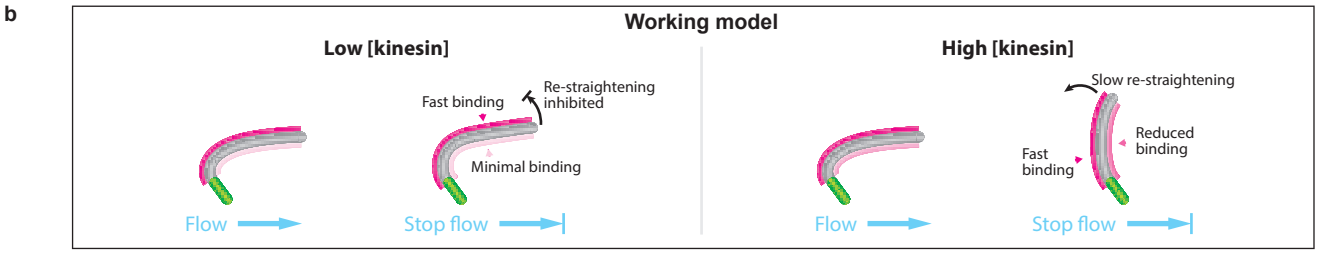

Figure 4 | Nucleotide-free motor domains can bend-lock microtubules. a, Time-lapse images of microtubule bending experiments for a range of kinesin concentrations. Blue arrows highlight the presence and direction of fluid flow. Dynamic microtubules appear white (dark-field) and fluorescent seeds are marked in green (epi-fluorescence). Each condition was tested twice on independent occasions. Microtubules shown here have been selected for having similar orientations. A more extensive selection is given in Supplementary Movie 2, which shows a complete range of orientations and lengths. The phenomenon is true for microtubules of comparable lengths, as can be seen in the movie. Scale bar: 5 μm. **b,** Working model. We predict that kinesin has a greater affinity for the expanded (convex) side of the microtubule lattice, and stabilises this lattice expansion. At high concentrations, the convex side of the microtubule will tend to saturate with kinesins, while recruitment to the concave side will continue slowly, driven by the higher concentration. As this continues, we envisage that it will cause the microtubule to re-straighten.

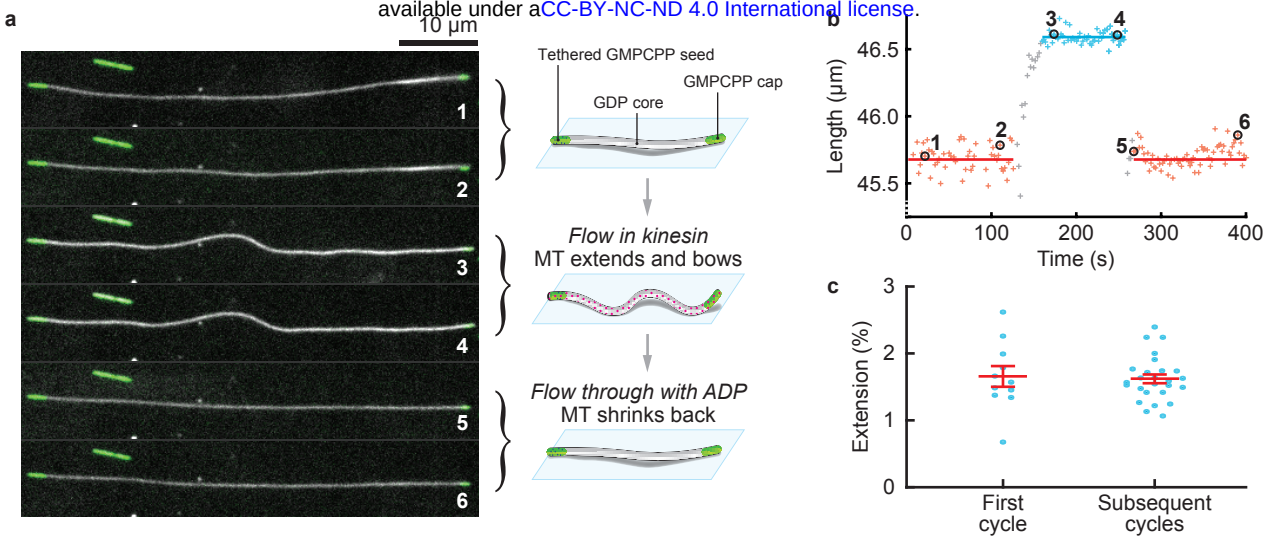

Figure 5 | Kinesin binding reversibly increases the lattice spacing of GDP-microtubules. a, GDP-microtubules (white) were grown from stabilised, green-fluorescent GMPCPP-tubulin seeds and stabilised similarly at their exposed tips. Seeds are tightly tethered to the surface via biotin-streptavidin linkages, whereas the rest of the microtubule is largely free to move (1,2). Flowing kinesin into the channel causes the microtubule to expand and additionally bow due to being pinned sparsely to the surface (3,4). Flushing with ADP-containing buffer encourages detachment of kinesin from the microtubule and also washes out kinesin molecules in solution. The microtubule then quickly reverts to its original length (5,6). Further detail can be seen in Supplementary Movie 3, which also shows a second expansion-contraction cycle. **b,** Length change of the GDP-part of the microtubule during a kinesin-induced extend-recoil cycle. Measurements are taken from the microtubule as shown in a and numbering corresponds to the frames shown. Horizontal lines show the mean length values in each phase. **c,** Relative extension of GDP-microtubules upon binding kinesin, categorised by the number of expansion-contraction cycles undertaken. Each point represents a different microtubule (no individual microtubule appears in each category). Mean ± standard error (*n*) is 1.66 ± 0.15 (11) for the first cycle, 1.62 ± 0.07 (26) for subsequent cycles and 1.63 ± 0.06 (37) for the total population. Mean values are not significantly different (p = 0.80, two-tailed t-test).